Int. J. Electrochem. Sci., 15 **(2020)** 7203 – 7213, doi: 10.20964/2020.08.05

International Journal of
ELECTROCHEMICAL
SCIENCE
www.electrochemsci.org

Excellent Cyclic Stability of Pre-lithiated VO_2(B) Nanorods as a Cathode Material for Lithium Ion Batteries

Shuchao Zhang, Zhengguang Zou, Tingting Lv, Shengyu Li, Yanjiao Zhang*

College of Materials Science and Engineering, Guilin University of Technology, Guilin, China.
*E-mail: zouzgglut@163.com

Received: 1 March 2020 / *Accepted:* 30 April 2020 / *Published:* 10 July 2020

Two-dimensional pre-lithiated VO_2(B) nanorods have been prepared via a facile hydrothermal method with vanadium pentoxide (V_2O_5), lithium nitrate ($LiNO_3$) and maltose($C_{12}H_{22}O_{11}$) as raw materials. The crystal structure and micromorphology of the prepared sample were characterized by XRD, FESEM, TEM, SAED, BET, Raman spectroscopy, and XPS. It revealed that pre-lithiation significantly reduced its thickness (10-20 nm), and showed a more regular rectangular plane at the display. Furthermore, the lithium storage performance of the sample was investigated through CV, EIS, and charge/discharge tests. The results manifested that the pre-lithiated VO_2(B) exhibited a much-enhanced electrochemical performance. For instance, the capacity retention rate of pre-lithiated VO_2(B) is 72.7% after 100 cycles at 0.1C, significantly higher than that (43.8%) of the pure VO_2(B). The improvement of the cycle performance of VO_2(B) after pre-lithiation can be mainly attributed to its excellent structural reversibility, shortened lithium ion transmission distance and enhanced electrical conductivity. The pre-lithiation method provides an insight to improve the cyclling performance of lithium-ion batteries.

Keywords: Lithium ion battery; Hydrothermal method; Pre-lithiated VO_2(B); Cycle performance.

1. INTRODUCTION

Rechargeable lithium-ion batteries (LIBs) have been widely used in portable electronic devices, electric vehicles, and smart grids owing to their large capacity, high energy density, and long cycle life[1-3]. Improving the electrochemical performance of cathode materials is the key to making breakthrough in LIBs[4]. Compared with traditional lithium ion battery cathode materials (such as $LiFePO_4$[5] , $LiCoO_2$[6], $Li_3V_2(PO_4)_3$[7]), Vanadium oxides (such as V_2O_5[8], V_3O_7[9], VO_2(B)[10]) has received extensive attention and in-depth research due to its advantages of high energy density, low cost, and easy synthesis. Among them, the metastable monoclinic VO_2(B) consists of double-layer V_4O_{10} with tunnels for rapid insertion/extraction of lithium ions, and has been recognized as a promising cathode material

for LIBs[11]. Unfortunately, the poor cycle performance of VO_2(B) greatly restricted its practical application in LIBs. Pre-lithiation can effectively complement the lithium ion depletion of the lithium ion battery in the chemical synthesis process, and improve the cyclling performance of the battery. Tian[12] synthesized pre-lithiated V_6O_{13} nanosheets by performing low-temperature stripping under a nitrogen atmosphere and performing secondary hydrothermal, and achieved excellent electrochemical performance. Lv[13] prepared a flower-shape V_6O_{13} via a simple solvothermal method, and the sample showed a capacity retention rate of 97% after 50 cycles. However, there have been few reports on pre-lithiation of VO_2(B) in recent years.

In order to improve the cycle performance of VO_2(B), herein, we report a facile hydrothermal method to synthesize pre-lithiated VO_2(B) nanorods. The microstructure and lithium ion storage performance of the pre-lithiated VO_2(B) nanorods have been analyzed by XRD, FESEM, TEM, SAED, XPS, Raman spectroscopy, BET, CV, EIS, and charge-discharge tests.

2. EXPERIMENTAL

2.1 Synthetic process

The pre-lithiated VO_2(B) nanorods were directly fabricated by a one-step hydrothermal method. First, 0.5 g of V_2O_5, 0.3 g of $C_{12}H_{22}O_{11}$, and 0.06 g of $LiNO_3$ were dissolved simultaneously in 50 ml of deionized water with vigorously stirring for 0.5 h. Hereafter, the solution was transferred to a drying box, and hydrothermally reacted at a temperature of 180°C for 24 h. After cooling to room temperature, the obtained precipitate was washed 3 times with deionized water. Finally, the precipitate was freeze-dried and calcined at 350°C for 1 h to obtain the final pre-lithiated VO_2(B) product. For comparison, the same process was used to synthesize the pure VO_2(B) cathode material but without adding $LiNO_3$.

2.2 Material characterizations

The phase structure of the samples were characterized by X-pert PRO-type X-ray diffraction(XRD) with Cu-K as the target at a scan rate of 10° per minute. The Field emission scanning electron microscopy (FESEM) morphology information was collected by a field emission scanning electron microscope model S-4800. The acceleration voltage was 20 KV and the maximum magnification was 500,000 times. Transmission electron microscopy (TEM) images were obtained using a FEI TECNALG2 high-resolution transmission electron microscope at an acceleration voltage of 200 kV. Raman spectroscopy data measurement was carried out using LabRAM HR Evolution of HORIBA, France. The specific area and porosity of the samples were analyzed by measuring of N_2 sorption at 77 K on Coulter SA 3100 instrument. The valence states of elements in the samples were analyzed by a INCA IE 350 X-ray photoelectron spectroscopy (XPS).

2.3 Electrochemical test

The electrochemical performance of samples were tested in CR2032 coin-type cells at room temperature. First, the as-prepared sample, acetylene black, and polyvinylidene fluoride (PVDF) were mixed in a weight ratio of 7: 2: 1 in N-methylpyrrolidone solvent to form a homogeneously slurry. Second, the slurry was uniformly coated on an Al foil substrate. Third, the coated Al foil was dried in a vacuum oven at 90 °C for 12 hours. Finally, the dried electrode sheet was cut into discs with a diameter of 16 mm.The coin cells were assembled in an argon-filled glove box with lithium metal foil as a counter electrode, Celgard 2300 film was used as a separator, and 1 M LiPF6 was dissolved in ethylene carbonate (EC) and dimethyl carbonate (DMC) in a volume ratio of 1: 1 as an electrolyte. Constant current charge-discharge cycle test was performed on A BTS Neware battery tester. Electrochemical impedance spectroscopy (EIS) and cyclic voltammetry (CV) were recorded by electrochemical workstation (CHI 860D), the frequency range of the EIS test is 0.01-10000 Hz.

3. RESULTS AND DISCUSSION

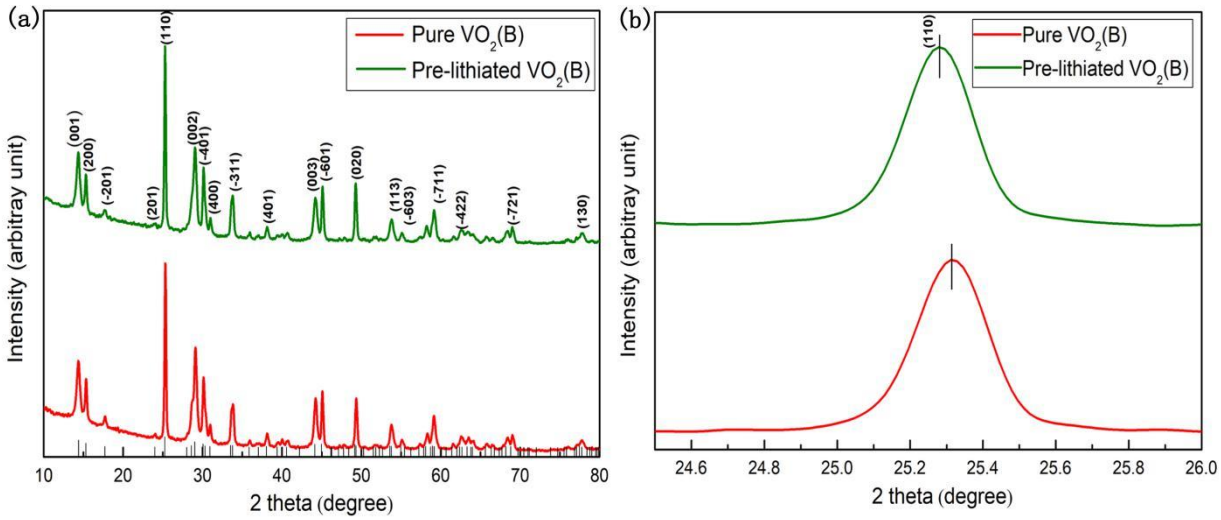

Figure 1. (a) The XRD patterns and **(b)** (110) crystal plane diffraction peak of the pure VO_2(B) and pre-lithiated VO_2(B) samples.

Table 1. Lattice parameters and unit cell volume of the pure VO_2(B) and pre-lithiated VO_2 (B) samples.

Sample designation	a(Å)	b(Å)	c(Å)	Volume(Å^3)
Pure VO_2(B)	12.0730	3.6913	6.4085	273.19
Pre-lithiated VO_2(B)	12.0748	3.6975	6.4352	274.74

The XRD diffraction patterns of the pure VO_2(B) and pre-lithiated VO_2(B) are shown in Figure 1. It can be seen that all the peaks of the two samples can be indexed to the monoclinic VO_2(B) (JCPDS NO. 81-2392)[14]. No impurity phase was detected, indicating that pre-lithiation did not change the crystal structure of VO_2(B). It should be noted that the (110) diffraction peak of the pre-lithiated VO_2(B) shifted to low angle as compared to the pure VO_2(B) (Figure 1(b)). From the XRD patterns, one can

draw the following conclusions: (i) Lithium ions have successfully entered the VO_2(B) unit cell in the chemical synthesis process after pre-lithiation; (ii) Lithium ions entering the VO_2(B) unit cell may cause the VO_2(B) lattice to expand, increase the interlayer distance of VO_2(B), and cause the diffraction peak to shift to a lower angle. **Table 1** compares the crystal parameters of the pre-lithiated VO_2(B) and pure VO_2(B). After pre-lithiation, the unit cell volume of VO_2(B) was enlarged, which facilitated the diffusion of lithium ions during cycling[15], the results are consistent with those in Figure 1 (b).

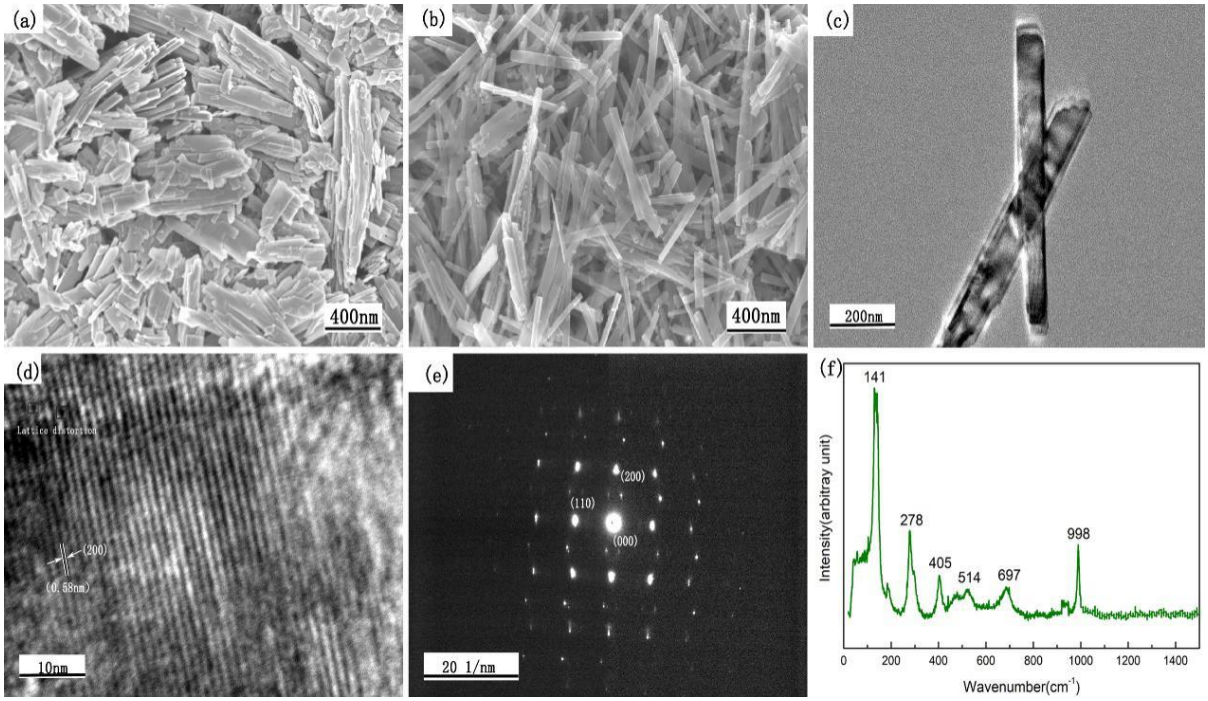

Figure 2. SEM images of the **(a)** pure VO_2(B) and **(b)** pre-lithiated VO_2(B) samples. **(c)** TEM, **(d)** HRTEM, **(e)** SAED and **(f)** Raman spectrum of the pre-lithiated VO_2(B) sample.

Figure 2 gives the SEM images of the pure VO_2(B) and the pre-lithiated VO_2(B) samples. It can be seen that the pure VO_2(B) sample consists of nanorods with different lengths and sizes (figture 2(a)); After lithiation (figture 2(b)), the nanorods morphology remains, but the thickness of the nanorods decreased significantly and the rectangular viewing angle became more obvious (the width ranges from 80 nm to 200 nm). Compared with the pure VO_2(B), pre-lithiated VO_2(B) has a smaller size, which also means a larger specific surface area[16], so that it is more conducive to the transfer of lithium ions.

In order to better observe the structure of the material, a single nanorod observed through TEM was shown in Figure 2(c). It can be seen that the width of the nanosheet is about 100 nm, which is in accordance with the FESEM images, indicating that VO_2(B) has a good sheet structure after pre-lithiation. In addition, HRTEM images and selected area electron diffraction images of the pre-lithiated VO_2(B) were also observed. As shown in Figures 2 (d) and (e), the distance between two adjacent lattice stripes is 0.58 nm, which corresponds to the distance between the two (200) crystal planes of VO_2(B). Of note, we also noticed some point defects, which indicated that the pre-lithiation process may cause the structure of the pre-lithiation VO_2(B) to undergo lattice distortion in advance and lithium ions occupy

different positions. The selected area electron diffraction is in good agreement with the XRD results[17,18].

The pre-lithiated VO_2(B) in the 0-1400 cm^{-1} wavelength range was shown in Figure 2 (f), which helped us understand its chemical and structural information. The Raman spectrum was occupied by peaks at 141 cm^{-1}, 278 cm^{-1}, 405 cm^{-1}, 514 cm^{-1}, 697 cm^{-1}, and 998 cm^{-1}, respectively. The bands at 141cm^{-1} and 278cm^{-1} can be attributed to the V–O–V bending mode and the outward pattern, respectively (bending/swaying). The bands at 405 cm^{-1} and 514 cm^{-1} can be ascribed to the V–O–V stretch pattern. The peak at 697cm^{-1} can be attributed to the coordination of the vanadium atom with three oxygen atoms, while the peak at 999cm^{-1} is due to the V=O stretching of distorted octahedral and distorted square-pyramids. According to the previous literatures[19-21], all these Raman peaks can be indexed to VO_2(B) vibrational bands, suggesting that the pre-lithiation has no significant effect on the type of chemical bonds in VO_2(B).

.

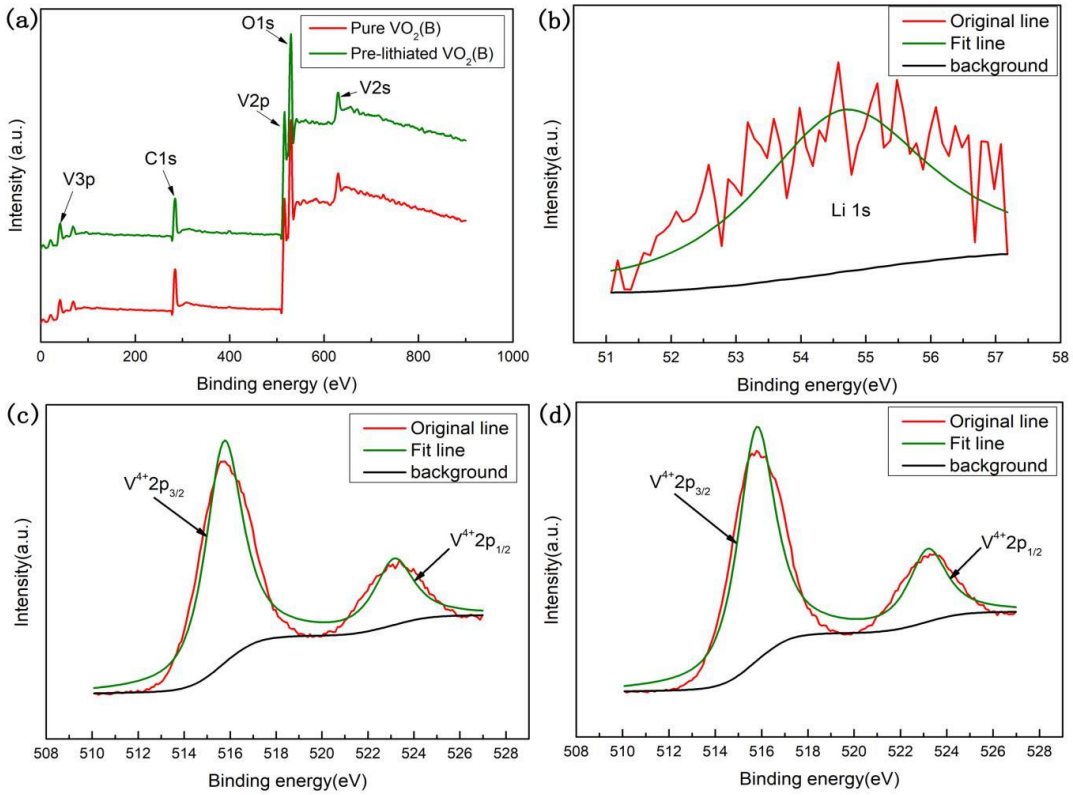

Figure 3. (a) Overall XPS spectra of the pure VO_2(B) and pre-lithiated VO_2(B) samples. **(b)** Li 1s XPS spectra of the pre-lithiated VO_2(B) sample. V 2p3/2 and V 2p1/2 XPS spectra of the **(c)** pure VO_2(B) and **(d)** pre-lithiated VO_2(B) samples.

Table 2. The binding energy of V^{4+} and V^{5+} of pure VO_2(B) and pre-lithiated VO_2(B).

Sample designation	Binding energy (eV)	
	V^{4+} $2p^{1/2}$	V^{4+} $2p^{3/2}$
Pure VO_2(B)	523.18	515.77
Pre-lithiated VO_2(B)	523.14	515.73

The elemental composition and valence of the samples could be characterized using X-ray photoelectron spectroscopy (XPS). The XPS overall spectra of the pure VO_2(B) and pre-lithiated VO_2(B) have been depicted in Figure 3(a). One can clearly see the peaks of C, O, and V elements in both samples. The peak of the C element comes from the residual organic matter, which is generated by the carbonization of the reducing agent during the reaction. The peak of Li element was not found in the overall spectrum, but we found the characteristic peak of Li 1s (Figture 3(b)) at the binding energy of 54.8 eV[22]. Then combined with the XRD pattern, no characteristic peaks related to Li were found. Therefore we could further infer that lithium ions have successfully entered the VO_2(B) lattice. Figure 3 (c) and (d) are the high-resolution V 2p XPS spectra of the pure VO_2(B) and pre-lithiated VO_2(B), respectively. As shown in Figure 3 (c), the binding energies of the two peaks at 515.77 V and 523.18 V for the pure VO_2(B) can be distributed to V^{4+} $2p^{3/2}$ and V^{4+} $2p^{1/2}$ respectively. Analogously, the two peaks at 515.73 V and 523.14 V for the pre-lithiated VO_2(B) can be ascribed to V^{4+} $2p^{3/2}$ and V^{4+} $2p^{1/2}$, separately. Regarding the V 2p binding energies of the two samples, we have listed them in **Table 2** respectively[23,24]. It can be learned that after pre-lithiation, the binding energy at V 2p moves to a lower direction, and according to the fitting result, the V element has only a valence of +4, indicating that the chemical environment may have changed resulting in a low binding energy[25]. The above results proved that lithium ions have been successfully pre-embedded in the VO_2(B) lattice.

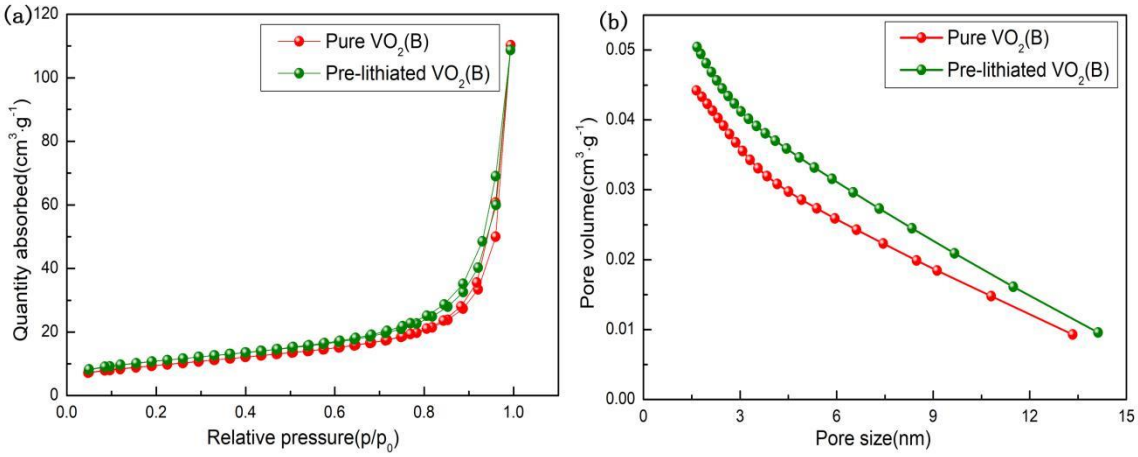

Figure 4. (a) N_2 adsorption-desorption isotherm curves and **(b)** pore size distribution curve of the pure VO_2(B) and pre-lithiated VO_2(B) samples.

Table 3. Specific surface areas and pore volume of the pure VO_2(B) and pre-lithiated VO_2(B).

Sample designation	Specific surface areas(m^2/g)	Pore volume(cm^3/g)
Pure VO_2(B)	33.37	0.044
Pre-lithiated VO_2(B)	38.03	0.053

Figure 4 presents the N_2 adsorption-desorption isotherms and pore size distribution curves for the two samples. It can be realized that the isotherm shows a typical IV isotherm and has a hysteresis loop, suggesting that the sample has a mesoporous structure. In addition, the type of hysteresis loop is H3 type, which indicated that the sample is composed of flakes or granules[15,26]. It was further proved that pre-lithiation did not significantly change the shape of VO_2(B), which corresponds to the SEM images. The specific surface area and pore volume of the two different samples were listed in **Table 3**. The specific surface areas of the pure VO_2(B) and pre-lithiated VO_2(B) are 33.37 m^2/g and 38.03 m^2/g, respectively. Their porosities are 0.044 cm^3/g and 0.053 cm^3/g, respectively. Compared with the pure VO_2(B), both the specific surface area and pore volume of pre-lithiated VO_2(B) increased to some extent. The increased specific surface area and pore volume after pre-lithiation could facilitate the diffusion of lithium ions, thereby improving the conductivity of the material[27,28].

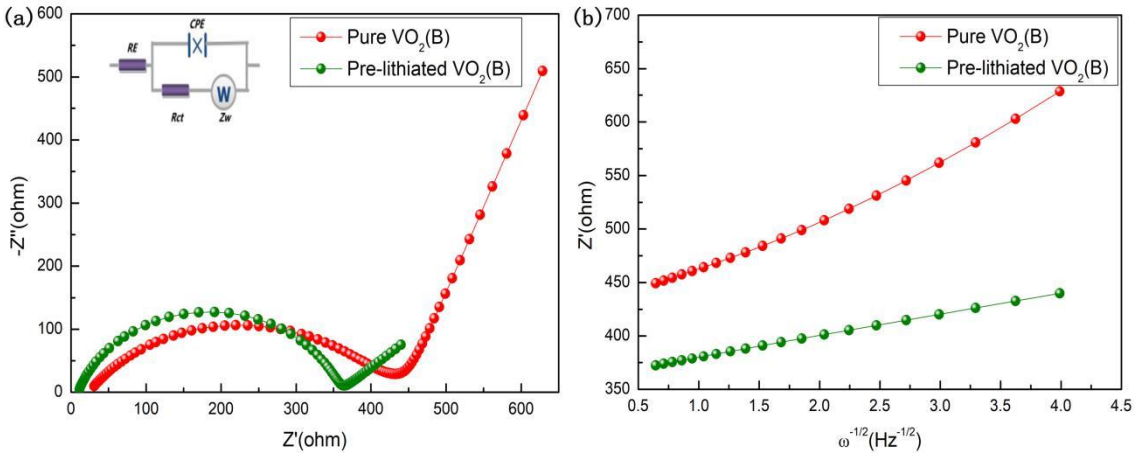

Figure 5. (a) Nyquist plots of the pure VO_2(B) and pre-lithiated VO_2(B). **(b)** The relationship between Z' and $\omega^{-1/2}$ in the low-frequency range.

Table 4. R_{ct} and D_{Li} values for pure VO_2(B) and pre-lithiated VO_2(B).

Sample designation	$R_{ct}(\Omega)$	D_{Li}（$cm^2\ s^{-1}$）
Pure VO_2(B)	438.7	4.14×10^{-15}
Pre-lithiated VO_2(B)	358.9	2.92×10^{-14}

In order to clearly understand the intercalation and de-intercalation of lithium ions in the active material[29], EIS spectra of the pure VO_2(B) and pre-lithiated VO_2(B) were shown in Figure 5 (a).The EIS plots are composed of a semicircle in the high frequency region and a straight line in the low frequency region, which represent the charge transfer resistance and lithium ion diffusion rate in the positive electrode material, respectively. The results showed that the charge transfer resistance (358.9Ω) of VO_2(B) was reduced after pre-lithiation compared with the charge transfer resistance (438.7Ω) of pure VO_2(B). This is because pre-lithiation increases the specific surface area of the material, provides more insertion positions for lithium ions, and improves capacity retention. Furthermore, the increase in the

porosity of the material also shortens the transmission distance of lithium ions, which in turn reduces the charge transfer resistance[17]. Then, the Warburg coefficient (σ) of the electrodes was obtained from the slope of the straight line Z'~ω-1/2(figure 5(b)), and the diffusion coefficient (D_{Li}) of lithium ions can be calculated by the following equation[30]:

$$D_{Li} = \frac{R^2T^2}{2A^2n^4F^4c^2\sigma^2}$$

R represents the gas constant (8.314 J mol^{-1} K^{-1}), T stands for Kelvin temperature (298 K), A is the relative area of the electrode material, n means the number of electrons transferred during the electrode reaction, and F is Faraday constant, c represents the concentration of the lithium ion phase, σ is Warburg coefficient. Afterward, the calculated values of the lithium ion diffusion coefficient and the charge transfer resistance of the sample were summarized in Table 4. The lithium ion diffusion coefficients of the pure VO_2(B) and pre-lithiated VO_2(B) are 4.14×10^{-15} cm^2 s^{-1} and 2.92×10^{-14} cm^2 s^{-1}, respectively. The lithium ion diffusion coefficient of pre-lithiated VO_2(B) was increased by almost an order of magnitude compared to the pure VO_2(B), this suggests that the pre-lithiated VO_2(B) is beneficial to improve the diffusion of lithium ions in VO_2(B).

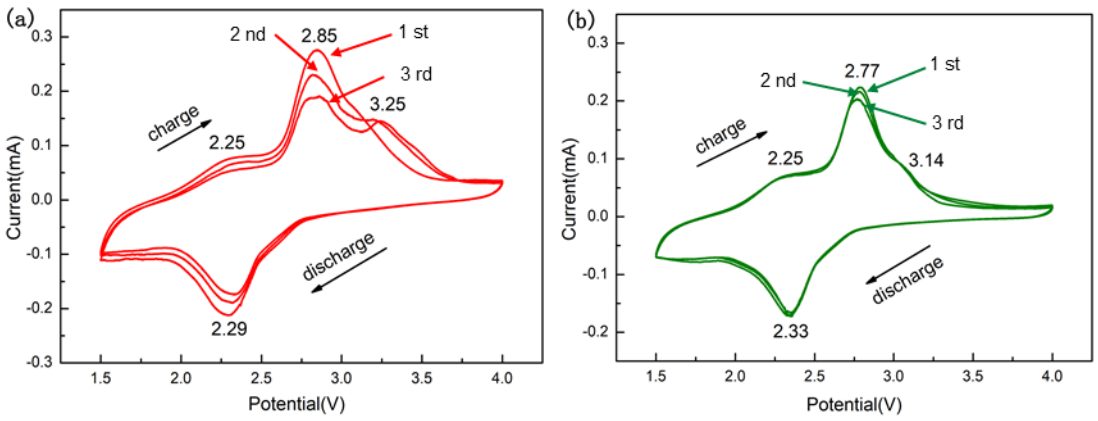

Figure 6. Cyclic voltammetry curves of **(a)** pure VO_2(B) and **(b)** pre-lithiated VO_2(B) at a scanning rate of 0.1 mV/s in the voltage range of 1.5–4.0 V.

To better explore the electrochemical performance of the pre-lithiated samples, three consecutive CV curves of the pure VO_2(B) and pre-lithiated VO_2(B) at a scanning rate of 0.1 mV/s in the voltage range of 1.5-4.0V were shown in the figure 6. The pure VO_2(B) has an intensive oxidation peak at 2.85V, and two weaker oxidation peaks at 2.25 V and 3.25 V, which represent the deintercalation of lithium ions process. There is a strong reduction peak at the position of 2.29 V, which represents the intercalation process of lithium ions. As shown in Figure 6 (b), the oxidation peaks at 2.85 V and 3.25 V are shifted to lower voltage, and the reduction peaks at 2.29 V are shifted to higher voltage. Furthermore, the CV curve of the sample corresponds well to its charge and discharge cycle results. Compared with the pure VO_2(B), the distance between the oxidation peak and the reduction peak of the pre-lithiated VO_2(B) becomes smaller, indicating that the symmetry of the two peaks is improved, which also proves that pre-lithiation is beneficial to extend the channel for intercalation and de-intercalation of lithium ions[31].

The overlapped CV curves after pre-lithiation shows that the additional phase of the sample is generated less, the reversible insertion of lithium ions is increased, and the material has excellent structural reversibility. The area of pre-lithiated VO_2(B) is slightly smaller than the pure VO_2(B), indicating that the initial discharge specific capacity of the sample decreased slightly after pre-lithiated[32,33].

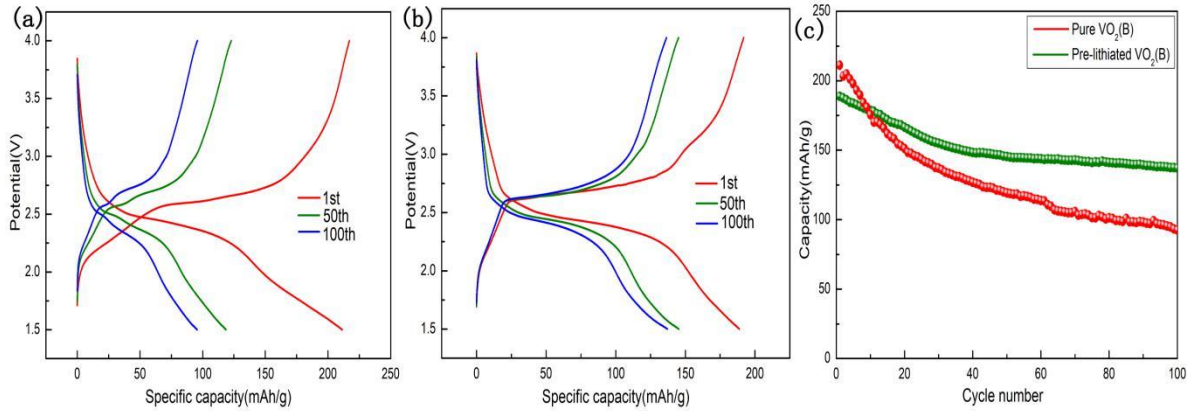

Figure 7. The first, fiftieth and hundredth charge and discharge curves of the **(a)** pure VO_2(B) and **(b)** pre-lithiated VO_2(B) at a current density of 0.1 C and a voltage range of 1.5-4.0 V. **(c)** Cyclic performance of the pure VO_2(B) and pre-lithiated VO_2(B) at a current density of 0.1 C and a voltage range of 1.5-4.0 V.

Table 5. Comparison of pre-lithiated VO_2(B) with similar cathode materials.

Cathode material	Capacity retention (%)/cycle number	Ref.
Fe-doped VO_2(B)	64.7/100	[14]
Ag-doped VO_2(B)	58.3/100	[25]
Al-doped VO_2(B)	71.6/50	[33]
Pre-lithiated VO_2(B)	72.7/100	This work

Figure 7 (a) and (b) give the first, 50th, and 100th charge-discharge curves of the pure VO_2(B) and pre-lithiated VO_2(B) at a current density of 0.1 C and a voltage range of 1.5-4.0 V. Both samples show obvious charging platforms at the position of about 2.7 V, and the discharge platform at the position of about 2.4 V. This result is in accordance with the CV curve. In addition, the length of the voltage platform is considered to be related to the kinetics of the redox reaction and the reversibility of the system[34]. The pre-lithiated charge-discharge platform is obviously longer than that of the pure VO_2(B), indicating that the reversibility of pre-lithiated VO_2(B) is better than the pure VO_2(B). The cycling performance of the sample at a current density of 0.1 C is shown in Figure 7 (c). Compared with the pure VO_2(B), the first discharge specific capacity of VO_2(B) after pre-lithiation is reduced, which may be caused by pre-lithiation. The conversion process allows lithium ions to enter the host lattice in advance

and occupy a large number of lithium ion positions, and also enables the host lattice to form a stable structure in advance[13]. Although the first discharge capacity of pre-lithiated VO_2(B) has been reduced, its cycle performance has been greatly improved. After 100 charge and discharge cycles, the capacity retention rate of pre-lithiated VO_2(B) is up to 72.7%, which is much higher than that (43.8%) of the pure VO_2(B), which is attributed to the lithium ion battery enhanced structural stability during charge and discharge, and improved lithium ion diffusion coefficient and electrical conductivity. At the same time, we have also listed similar cathode materials previously reported in Table 5. It can be clearly found that the cycle performance of pre-lithiated VO_2(B) is superior to other cathode materials.

4. CONCLUSION

In summary, pure and pre-lithiated VO_2(B) were prepared by a simple hydrothermal method. The pre-lithiated VO_2(B) nanorods have a more regular rectangular viewing angle than the pure VO_2(B). Electrochemical tests demonstrated that when the molar ratio of Li/V is 0.16, the capacity retention rate of the pre-lithiated VO_2(B) is up to 72.7% after 100 charge-discharge cycles, increasing by 28.9% compare to pure phase. The much improved cycling performance of the pre-lithiated VO_2(B) can be attributed to the following aspects: (i) after pre-lithiation, lithium ions are embedded in VO_2(B) lattice in advance, which expands the unit cell volume, reduces the charge transfer resistance, and facilitates the diffusion of lithium ions in VO_2(B), thereby improving its cycling performance; (ii) during the pre-lithiation process, fewer additional phases are generated in the sample, which leads to an increase in the electrochemical reaction reversibility, thereby giving the material excellent structural reversibility; (iii) the increased specific surface area and porosity reduced the diffusion distance of lithium ions and improved the conductivity of the material.

ACKNOWLEDGEMENT
This work was supported by the National Nature Science Foundation of China (No.51562006)

References

1. Z.G. Zou, S.C. Zhang and S.Y. Li, *Mater. Technol.,* 35 (2020) 300.
2. P. Wang, J.J Xu, F. Xu, W. Zhao, P. Sun, Z.C. Zhang, M. Qian and F.Q. Huang. *Carbon.,* 134 (2018) 391.
3. H. Sitinamaluwa, S.Q. Zhang, W. Senadeera, G. Will and C. Yan, *Mater. Technol.,* 31(2016) 872.
4. H.L. Wang, Y. Yang, Y.Y. Liang, J.T. Robinson, Y.G. Li, A. Jackson. Y. Cui and H.J. Dai. *Nano Letters.,* 11 (2011) 2644.
5. C.P. Hou, Y. Ma, H. Zhang, W.C. Geng and Q.Y. Zhang, *Mater. Technol.,* 33 (2018) 16.
6. J. Lu, K.S. Lee, *Mater. Technol.,* 31 (2016) 628.
7. X. You, S. Xiao, T. Zhang, D. Zeng, Q. Xiao, Z. Li and G. Lei, *Mater. Technol.,* 30 (2015) A64.
8. Y.L. Cheah, V. Aravindan and S. Madhavi, *J. Electrochem. Soc.,* 159 (2012) A273.
9. X.Y. Zhang, M.H. Yu, S.B. Zhao, F. Li, X.L. Hu, S.B. Guo, X.L. Lu and Y.X. Tong, *Part. Part.*

Syst. Char., 33 (2016) 531.
10. S. Lee, X. G. Sun, A.A. Lubimtsev, X. Gao, P. Ganesh, T.Z. Ward, G. Eres, M.F. Chisholm, S. Dai and H.N. Lee, *Nano letters.,* 17 (2017) 2229.
11. L.Q. Mai, Q.L. Wei, Q.Y. An, X.C. Tian, Y.L. Zhao, X. Xu, L. Xu, L. Chang and Q.J. Zhang, *Adv. Mater.,* 25 (2013) 2969.
12. X.C. Tian, X. Xu, L. He, Q.L. Wei, M.Y. Yan, L. Xu, Y.L. Zhao, C.C. Yang and L.Q. Mai, *J. Power Sources.,* 255 (2014) 235.
13. T.T. Lv, Z.G. Zou, Y.W. Li and S.C. Zhang, *Ionics.,* 26 (2020) 1181.
14. Z.G. Zou, S.C Han, Y.W. Li, X.Y. Wu, Q. Yang and T.T. Lv, *Int. J. Electrochem. Sci.,* 13 (2018) 8127.
15. Y.J. Zhang, Z.G. Zou, J. Liu, S.C. Zhang and H.H. Zhang, *Mater. Technol.,* (2020).
16. A.S. Yu, Kumagai N, Z.L. Liu and J.Y. Lee, *J. Power Sources,* 74 (1998) 117.
17. S.Y. Li, Z.G. Zou, Y. Li, Y.J. Zhang and H.H. Zhang, *J. Electroanal. Chem.,* 857 (2020).
18. L.Q. Mai, B. Hu, T. Hu, W. Chen and E.D. Gu, *J. Phys. Chem. B,* 110 (2006) 19083.
19. S.B. Ni, H.H. Zeng and X.L. Yang, *J. Nanomater.,* (2011).
20. J. Twu, C.F. Shih, T.H. Guo and K.H. Chen, *J. Mater. Chem.,* 7(1997) 2273.
21. X.C. Wu, Y.R. Tao, D. Lin, Z.H. Wang and H. Zhang, *Mater. Res. Bull.,* 40(2005) 315.
22. K. West, B. Zachau-Christiansen, T. Jacobsen and S. Atlung, *J. Power Sources,* 14 (1985) 235.
23. X.H. Liu, G.Y. Xie, C. Huang, X. Qian, Y.F. Zhang and Y.B. Luo, *Mater. Lett.,* 62 (2008) 1878.
24. B. Horvath, J. Strutz, J. Geyer-Lippmann and E.G. Horvath, *chem. Information.,* 13(1982).
25. S.C. Han, Z.G. Zou, T.T. Lv, X.Y. Wu and Q. Yang, Chin. *J. Chem. Eng.,* 69 (2018) 495.
26. R. Schmidt, M. Stöcker, E. Hansen, D. Akporiaye and O.H. Ellestad, *Microporous Mater.,* 3 (1995) 443.
27. Y.C. Liu, W. Naelih and W.R. Liu, *J. nanosci. Nanotechnol.,*18(2018) 68.
28. Q. Yang, Z.G. Zou, X.Y. Wu, Y.J. Zhang and S.Y. Li, *J. Chin. Ceram. Soc.,* 47 (2019) 1670.
29. D.W. Liu, Y.Y. Liu, A.Q. Pan, K.P. Nagle, G.T. Seidler, Y.H. Jeong and G.Z. Cao, *J. Phys. Chem. C*, 115 (2011) 4959.
30. J.Y. He, F. Long, Z.G. Zou, W.M. Wang and Z.Y. Fu, *Ionics*, 21 (2015) 995.
31. X.Y. Wu, Z.G. Zou, S.Y. Li and Q. Yang, *J. Electroanal. Chem.,* 829 (2018) 20.
32. S. Luo, K. Wang, J.P. Wang, K.L. Jiang, Q.Q. Li and S.S. Fan, *Adv. Mater.,* 24 (2012) 2294.
33. Z.G. Zou, Z.L. Hou, J.L. Wang, Y. Gao, Z.D. Wan and S.C. Han, *Int. J. Electrochem. Sci.,* 12 (2017) 4979.
34. X.W. Zhou, G.M. Wu, G.H Gao, J.C. Wang, H.Y. Yang, J.D. Wu, J. Shen, B. Zhou and Z.H. Zhang, *J. Phys. Chem. C,* 116 (2012) 21685.